Clean Technologies and Environmental Policy (2019) 21:121–138
https://doi.org/10.1007/s10098-018-1622-3

ORIGINAL PAPER

Performance of γ-aluminium oxide nanoparticles for arsenic removal from groundwater

Somaparna Ghosh[1] · Roshan Prabhakar[1] · S. R. Samadder[1]

Received: 6 June 2018 / Accepted: 3 October 2018 / Published online: 11 October 2018

Abstract

The present study aims to investigate the applicability of γ-Al_2O_3 nanoparticles (NPs) adsorbent for removal of arsenite and arsenate from aqueous solution. The nano-adsorbent was characterized using zeta potential analysis, dynamic light scattering, field emission scanning microscopy, energy-dispersive X-ray spectroscopy, Fourier transform infrared spectroscopy and X-ray diffraction. Batch adsorption studies were carried out to optimize adsorption parameters such as contact time, stirring speed, initial arsenic concentration, adsorbent dose, pH and effect of different competing anions. Langmuir adsorption capacities obtained at 298 K are 769.23 µg/g and 1000 µg/g for As(III) and As(V) removal correspondingly. The adsorption mechanism was well established by pseudo-second-order kinetic model. Negative values of enthalpy (ΔH°) obtained during adsorption [− 29.12 kJ/mol and − 35.55 kJ/mol for As(III) and As(V), respectively] confirmed the process was exothermic in nature. The negative values of ΔG° [− 6.14 to − 3.86 kJ/mol for As(III) and − 9.32 to − 6.68 kJ/mol for As(V)] further affirmed that the adsorption process is spontaneous in nature. There was no requirement of additional external energy supply for the enhanced removal as the adsorption was less favoured at high temperature. Phosphate and sulphate had the profound effect on reduction in the removal efficiency. Good regenerating efficiency of γ-Al_2O_3 NPs up to fourth cycle implied economic feasibility of the adsorbent. The effectiveness of γ-Al_2O_3 was also proved for removal of arsenic from real arsenic-contaminated groundwater.

Electronic supplementary material The online version of this article (https://doi.org/10.1007/s10098-018-1622-3) contains supplementary material, which is available to authorized users.

✉ S. R. Samadder
samadder@iitism.ac.in; sukh_samadder@yahoo.co.in

[1] Department of Environmental Science and Engineering, Indian Institute of Technology (Indian School of Mines), Dhanbad 826004, India

Graphical abstract

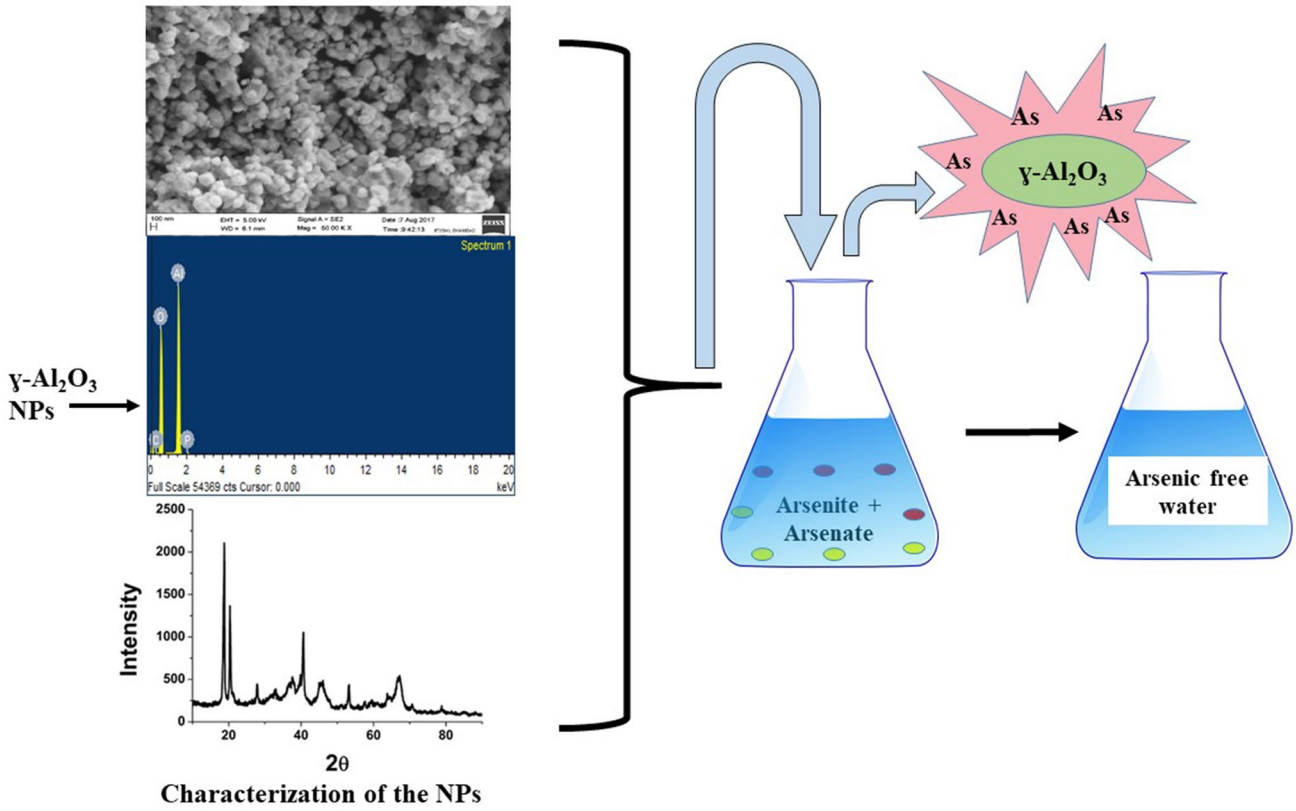

Keywords Adsorption · Arsenate · Arsenite · γ-Al_2O_3 nanoparticles · Isotherm models · Field application

Introduction

Groundwater contamination due to the presence of different heavy metals is a major global concern of recent times. Among the various heavy metals present in groundwater, arsenic possesses maximum health risk through consumption of arsenic-contaminated drinking water. Around the globe, almost 200 million people from 105 countries are affected with the arsenic contamination (Murcott 2012; Naujokas et al. 2013). 85% of the Indian population rely on groundwater to meet their domestic requirements (Roy et al. 2015). South Asian countries such as Vietnam, Bangladesh, China and India are suffering from severe arsenic toxicity due to their natural geological condition (Inaba et al. 2016) and existence of arsenic-bearing minerals in the local bed rocks (Garelick et al. 2009). India and Bangladesh are greatly affected by this menace of groundwater arsenic contamination (Chakraborti et al. 2017). The study conducted by Chakraborti et al. (2016) reported that about 70 million population in India are at risk of consuming arsenic-contaminated water above WHO guideline value of 10 µg/L. Arsenic gets into sub-surface environment via oxidation of arsenopyrite minerals and disintegration of arsenic-containing iron oxy-hydroxide (FeOOH) in reducing conditions (Bose and Sharma 2002). Arsenite and arsenate are two inorganic forms of arsenic which are found to be present in natural groundwater and sediments. Of these two forms, arsenate is less toxic than the trivalent arsenite. Several epidemiological studies have affirmed the adverse health effects such as dermal effects (Chowdhury et al. 2000; Mukherjee et al. 2005), cardiovascular disorder (Wang et al. 2007), respiratory ailments (Mazumder et al. 2000) gastrointestinal effects (Rahman et al. 2001), endocrinological malfunctioning (diabetes mellitus) (Chen et al. 2007), neurological disorder (Mukherjee et al. 2003, 2005), reproductive and developmental disorder (Chakraborti et al. 2003) and cancer (Rahman et al. 2009). Arsenic has been categorized as Class A human carcinogen (Dutta et al. 2004). It has been reported that the drinking of arsenic-laden water having arsenic concentration more than 50 µg/L can cause death due to cancer in 13 out of 1000 population exposed (Smith et al. 2002). People from rural areas with poor economic background

are most affected from groundwater arsenic toxicity as they are unable to afford costly water treatment systems. It is important to find an economical and simple way to provide arsenic-free drinkable water to the rural communities of India as they are the severely affected ones with this deeply rooted menace of groundwater contamination.

Numerous technologies have been used so far for removal and remediation of arsenic from groundwater such as oxidation–precipitation (Leupin and Hug 2005), coagulation and flocculation (Hansen et al. 2006), filtration techniques using membranes like reverse osmosis, ion exchange (Ning 2002) and nano-filtration (Kim et al. 2006). Major drawbacks associated with these conventional methods are involvement of high capital investment, excessive production of sludge, membrane dysfunction due to clogging over time and continuous monitoring of ion concentration (Owlad et al. 2009). In contrast to the disadvantages of the above techniques, adsorption is considered as one of the most suitable, competent and economical methods for arsenic remediation from aqueous solution (Goswami et al. 2012). However, asymmetrical pore structure and low surface area of most of the traditional adsorbents cause low adsorption and removal capacities limit their uses in large-scale application (Prabhakar and Samadder 2018). Development of nano-adsorbents has enabled the objective of advancement of adsorbents which have enormous surface area and massive amount of active sites that facilitate better arsenic removal efficiency compared to other available adsorbents and do not produce toxic substances during arsenic adsorption. Nanoparticles are 5–10 times more efficient adsorbent for removing arsenic than their micron size counterparts (Ponder et al. 2001; Sharma et al. 2009). Different metal oxide-based nanoparticles such as iron oxides/hydroxides, titanium oxides, oxides of copper, zirconium oxide and mixed metal oxides have been explored and used by the researchers globally for arsenic removal (Lata and Samadder 2016). Aluminium-based nano-adsorbents are drawing more attention of researchers as they are economical from manufacturing aspect and have high decontamination ability (Giles et al. 2011). The reason for its extensive use for different applications lies behind its unique features like greater surface area, high surface reactivity and more surface binding energy. Aluminium-based materials are found in different forms and phases. Of these, gamma phase has added structural properties and improved thermodynamic stability due to its attainment of critical surface area. Generally, nano-alumina has a pH_{ZPC} value above the 7.5, which provides an added advantage for removal of anionic contaminants in neutral pH range. There are three possible mechanisms for metal ions adsorption using γ-Al_2O_3: (1) metal ion adsorption by some specific functional group, (2) hydrolyzation of metal ion and (3) electrostatic attraction. So far, γ-alumina has been extensively used for dyes and other heavy metals removal from wastewater. There are very few reports on the use of γ-alumina for arsenic removal from drinking water sources. Arsenite is predominant in anoxic condition, whereas arsenate is predominant when sufficient reducing condition prevails in groundwater and in vadose zone. In the available literature, the majority of the studies are focused on removal of either arsenite or arsenate from the aqueous environment. Alumina-based adsorption has been recommended as of the prominent available technologies for arsenic remediation from water by the leading agencies (USEPA 2000). Therefore, because of the involvement of cost for its large-scale application in arsenic removal from drinking water, γ-Al_2O_3 NPs efficacy needs to be tested in batch process at laboratory scale. Owing to the limitations of studies for removal of both the arsenic species simultaneously from the aqueous solution, the current study examined and used the unique properties of γ-aluminium oxide nanoparticles (γ-Al_2O_3 NPs) for arsenic (III and V) removal from groundwater. The present study elaborated all necessary inputs such as affecting parameters, isotherm models and detailed isotherm and kinetic parameters to check and understand the adsorption behaviour of γ-Al_2O_3 NPs. Further, it was also aimed to test its efficacy against the real field samples.

Materials and methods

Materials

All the chemicals comprising sodium arsenate (Loba Chemie, India), sodium arsenite (Loba Chemie, India) and aluminium oxide (Gamma) nanoparticles (Reinste, India) were of AR grade. Ultrapure deionized water was used for the sample preparation and thorough cleaning of the glasswares. All the chemicals were used without any modification.

Methods

Instrumentation

pH of samples was inspected using digital pH meter (Labman, India). Zero point charge (pH_{ZPC}) was determined by adding 0.05 g of nano-γ-aluminium oxide nanoparticles to the NaCl (0.01 M) solutions of diverse pH values, ranging from 2 to 12. The reaction mixtures were stirred using shaker at 150 rpm for 48 h to attain equilibrium. A graph of initial pH versus change in pH (ΔpH) values was plotted, and the point of intersection represented the pH_{ZPC} of the nano-adsorbent used in the present study. The zeta potential and hydrodynamic diameter of γ-Al_2O_3 nanoparticles were obtained using zeta potential analyser (LA-350, Horiba, Japan). The combined structure of the nanoparticles was broken down by sonicating the suspension using ultrasonic

bath (Wise clean, India) for 30 min prior to the dynamic light scattering (DLS) analysis. The surface morphological examination of the nano-adsorbent was conducted by field emission scanning microscopy (FESEM) (Supra 55, Carl Zeiss, Germany). The sample was attached to a metallic disc using carbon adhesive tapes during FESEM analysis. 10 kV was the operating voltage for recording the images at different magnifications. The elemental composition and purity analysis were done using EDX (energy-dispersive X-ray spectroscopy) accessory available with FESEM. Phase analysis of the nano-adsorbents was executed using X-ray diffraction (XRD) (D2 Phaser, 2nd Gen, Bruker, India). The source radiation of Cu-Kα for XRD analysis was 0.154 nm with the 2θ range of 10°–90°. The functional groups present in the raw and used adsorbent were identified using FTIR (Fourier transform infrared spectroscopy) (Spectrum 2000, PerkinElmer, USA).

Experimental design for adsorption study

Stock solutions of 1000 mg/L concentration of sodium arsenite ($NaAsO_2$) and sodium arsenate ($Na_2HAsO_4{\cdot}7H_2O$) were made. The working standard solutions were prepared by dilution for further studies. Batch parametric studies were done using 250-mL conical flask at room temperature (25 ± 2 °C). Incubator shaker (Rivotek, India) was used for agitating the samples during the study. For separation of nanoparticles after adsorption from aqueous solution, centrifuge (R-24, Remi Lab World, India) was used at 8000 rpm for 10 min. The parameters affecting the removal of arsenic species were optimized by fluctuating the contact time from 10 to 1400 min, stirring speed from 50 to 200 rpm and initial arsenic concentration from 50 to 400 µg/L. The assessment of equilibrium time for the current study was done with 100 µg/L arsenic concentration and 0.5 g/L of adsorbent dose. Other variables of the adsorption process, i.e. initial arsenic concentration, stirring speed, adsorbent dosage, pH and temperature, were kept constant. Time intervals of agitation of samples were varied from 10 min to 24 h. 50 mL samples of 100 µg/L solution with adsorbent dose of 0.5 g/L for both the arsenic species was taken to study the effect of stirring speed. Speed was varied with predetermined contact time of 120 min with fixed value of all other factors like initial arsenic concentration, adsorbent dose, pH and temperature. A fixed quantity of adsorbent was added to 50 mL of separately prepared samples of arsenite and arsenate for optimization of initial arsenic concentration. The samples were stirred at fixed speed of 150 rpm, and contact time was kept at 120 min for both arsenic species. The influence of the adsorbent dosage was observed by fluctuating the dose from 0.1 to 2 g/L keeping other remaining parameters fixed. pH and temperature were varied from 2–12 and 298–328 K during optimization study, respectively. During batch adsorption studies, the remaining concentration of arsenic was measured using atomic absorption spectrophotometer (AAS) (Avanta PM, GBC, Australia). For quality assurance and control, the instrument was calibrated using standard solutions before performing the experiments. The calibration curves were generated, and correlation coefficients values of 0.99 or more were obtained during each standardization procedure. A check solution of the known concentration was analysed after every 10th sample for examining the instrument performance. All the observations were recorded within 10% of relative standard deviation (RSD). Each experiment was triplicated, and the results that have been reported in the manuscript are the average values. For arsenate estimation, samples were pre-reduced as per the standard method. The removal efficiency and the uptake capacity of the γ-Al_2O_3 NPs were obtained using Eqs. (1) and (2):

$$\text{Removal } R(\%) = \frac{(C_o - C_e) * 100}{C_o} \tag{1}$$

$$Q_e = \frac{(C_o - C_e) * V}{m} \tag{2}$$

where C_o is initial concentration and C_e stands for concentration at equilibrium in µg/L. The equilibrium uptake capacity (µg/g) is represented by Q_e, and V symbolizes the volume (L) of samples. "m" denotes the quantity (g) of gamma-alumina used.

Adsorption isotherms

Adsorption isotherm models are well known and extensively used mathematical methods to analyse the adsorption capacity for removal of different contaminants. Isotherms play a significant part in intriguing the adsorption behaviour and analysing the uptake capacity of adsorbents. Most appropriate correlation for the equilibrium curves is established for design optimization of the removal of metal ions from effluents using sorption techniques (Kim et al. 2004). Langmuir and Freundlich isotherms models are frequently cast-off for adsorption process consisting of single solute. In the current study, adsorption isotherm studies were done at four different temperatures. Isotherm studies were conducted at four different temperatures of 298 K, 308 K, 318 K and 328 K with arsenic concentration of 300 µg/L, equilibrium time of 120 min and at pH of 6.8. The assumptions of Langmuir isotherm model are that all the active sites consist of equal activation energy and adsorption will only occur through monolayer coverage (Allen et al. 2004). A separation factor (R_L) which is dimensionless parameter, is used to understand the feasibility information of the adsorption studies (Weber and

Chakravorti 1974). Freundlich isotherm model elucidates physical adsorption on surfaces (homogenous and heterogeneous). It is also appropriate for mono- and multilayer adsorption studies (Khan et al. 2013). This isotherm model was incorporated in the present study as this model gives satisfactory results for moderate and high range of concentrations of pollutants. The type of interaction (physical and chemical adsorption process) between the adsorbate and adsorbent is examined through Dubinin–Radushkevich (D–R) isotherm model. Therefore, adsorption data set was also assessed using D–R isotherm model to know the bonding type between the arsenic species and γ-Al_2O_3 NPs. The values of the mean sorption energy (E) explain the kind of adsorption mechanism involved. Temkin isotherm provides important insights into the heat of adsorption and binding energy. The assumptions of Temkin model state that as a result of interaction between adsorbing element and adsorbate molecules, the heat of adsorption reduces linearly (Temkin and Pyzhev 1940). The linear mathematical expressions of the Langmuir isotherm, Freundlich isotherm, D–R and Temkin isotherm models are represented by Eqs. (3)–(9), respectively (Nassar et al. 2017; Tofik et al. 2016; Lin and Juang 2002; Chaudhry et al. 2016).

$$\frac{C_e}{Q_e} = \frac{1}{K_L Q_m} + \frac{C_e}{Q_m} \tag{3}$$

$$R_L = \frac{1}{1 + K_L C_o} \tag{4}$$

$$\log Q_e = \log K_f + \frac{1}{n} \log C_e \tag{5}$$

$$\ln Q_e = \ln Q_m - k\varepsilon^2 \tag{6}$$

$$\varepsilon = RT \ln\left(1 + \frac{1}{C_e}\right) \tag{7}$$

$$E = \frac{1}{\sqrt{(-2k)}} \tag{8}$$

$$Q_e = \frac{RT}{b_T} \ln A_T + \frac{RT}{b_T} \ln C_e \tag{9}$$

where C_e and Q_e have the standard meaning as stated above and Q_m is the maximum uptake capacity. Langmuir constant K_L represents the sorption energy. R_L is a dimensionless separation factor. The R_L values greater than 1 indicate unfavourable condition for adsorption process, whereas favourable condition prevails when R_L values fall between 0 and 1. The constants K_f and n in Eq. (5) symbolize the adsorption capacity and intensity of adsorption, respectively. k is average energy of adsorption required for per mole of the adsorbate. ε is Polanyi potential, which is defined by Eqs. (6) and (7), respectively. Mean free energy (E) is calculated using Eq. (8). R is the universal gas constant. T represents the temperature in K. A_T (L/g) is the equilibrium binding constant correlated with maximum binding energy and was found from the ln C_e and Q_e plot [Eq. (9)]. The constant b_T is associated with the heat of adsorption.

Kinetic study

Removal of arsenic from aqueous solution is a function of time, and it is crucial to determine the adsorption rate to design a process for field applications. Valuable information about the mechanism of sorption can be obtained through the study of the kinetic parameters. The efficiency of adsorption is governed by the uptake rate with respect to the contact time (Kim et al. 2004). Kinetic models were employed at particular time intervals ranging from 10 to 120 min with optimized arsenic concentration of 300 µg/L. 0.5 g/L and 0.75 g/L of adsorbent doses were added to the sample solutions at the equilibrium pH of 6.8 at 298 K. Pseudo-first-order, pseudo-second-order, intraparticle and liquid film kinetic models were applied for the present study. Pseudo-second-order kinetic model assumes sharing and trading electrons between adsorbate and adsorbent. Intraparticle diffusion describes that the diffusion of the adsorbate (solute) ions takes place through the interior pores of the adsorbents. Weber and Morris (1963) and Wen et al. (2014) suggested that this transportation is a rate-limiting step and adsorption changes proportionally with $t^{1/2}$. The liquid film diffusion model was applied to investigate whether the formation of external boundary layer is taking place during adsorption or not. The linearized forms of these models are represented by Eqs. (10)–(13) (Ho and McKay 1998; Kumar et al. 2011; Weber and Morris 1963; Boyd et al. 1947)

$$\log(Q_e - Q_t) = \log Q_e - \frac{k_1 t}{2.303} \tag{10}$$

$$\frac{t}{Q_t} = \frac{1}{k_2 Q_e^2} + \frac{1}{Q_e} \tag{11}$$

$$Q_t = k_{id} t^{\frac{1}{2}} + C \tag{12}$$

$$\ln(1 - f) = -k_{fd} t \tag{13}$$

where Q_e has the customary meaning. Q_t (µg/g) indicates the uptake capacity of γ-Al_2O_3 NPs at any time "t". k_1 is the pseudo-first-order rate constant. k_2 signifies the pseudo-second-order rate constant. k_{id} represents intraparticle diffusion rate constant. In Eq. (13), $f = Q_t/Q_e$ is related to the

partial acquirement of equilibrium and k_{fd} is the rate constant related to film diffusion.

Similarly, thermodynamic studies were executed by varying the temperature in between 298 and 328 K. Naturally, the groundwater contains several ions, which may affect the adsorption process. So, the impact of different anions on the adsorption of arsenite and arsenate such as bicarbonate, chloride, sulphate, nitrate, phosphate was also examined for the present study. Optimum dosage of gamma-alumina NPs was added to the reaction mixtures of arsenite and arsenate correspondingly. Regenerating efficiency of the nanoparticles (NPs) was also assessed to examine the economic feasibility of NPs in large-scale application. 0.5 N NaOH solution was used to regenerate the spent nano-adsorbent after each cycle of adsorption–desorption. Four adsorption–desorption cycles were carried out with initial concentration of 100 µg/L arsenite solution. In order to do the experiments with real groundwater, samples were collected from the hand pumps located in Badi Kudrijana village, Sahebganj, Jharkhand, India, during February 2018. Sampling was done after pumping out the water 30–40 times to avoid the partially oxidized water out of the tube well. Two sets of samples were collected for physicochemical and elemental analysis. The pH, TDS and EC of unacidified set of samples were measured on site at the time of sampling with digital pH meter. The remaining parameters were measured as per the standard method of APHA (APHA 2012). Arsenic and other heavy metals were measured using HG-AAS and FAAS, respectively.

Results and discussion

Characterization

It can be seen from the histogram analysis of Fig. 1a that the size varied in the range of 104–115 nm for the γ-alumina nanoparticles and average size was recorded as 111 nm. The zeta potential value of + 32.4 mV as shown in Fig. S2 represented moderate degree of stability of the γ-Al_2O_3 NPs in aqueous medium. It showed that γ-Al_2O_3 is uniformly stable in aqueous suspension and does not precipitate with time. Figure 1b and Fig. S1 show the morphological examination using FESEM and EDX. Most of the nanoparticles of γ-Al_2O_3 were spherical with size variation of 60–80 nm. The morphological features of the nano-adsorbent confirmed that the surface properties are quite suitable for adsorption phenomenon to take place. Elemental analysis confirmed the purity of the γ-Al_2O_3 NPs. EDX spectrum showed profound peaks for Al (38.86% by weight) and O (58.62% by weight), but a weak peak was observed for C (2.34% by weight). Al and O signals were due to aluminium oxide, and weak C signal was due to the use of carbon adhesive tapes for sample affixation during analysis. Very mild signal of P may be attributed to instrumental error as the equipment is for testing various other materials. The significant peaks, as shown in Fig. S3 at 2θ values of 19.45°, 31.93°, 37.60°, 39.49°, 45.86°, 60.89° and 67.03°, represent the respective crystal planes of γ-Al_2O_3, (111), (200), (311), (222), (400), (511) and (440) (Patra et al. 2012). Therefore, the XRD results of the powdered Al_2O_3 NPs showed the crystalline structure of the Al_2O_3 in gamma phase. The BET surface area

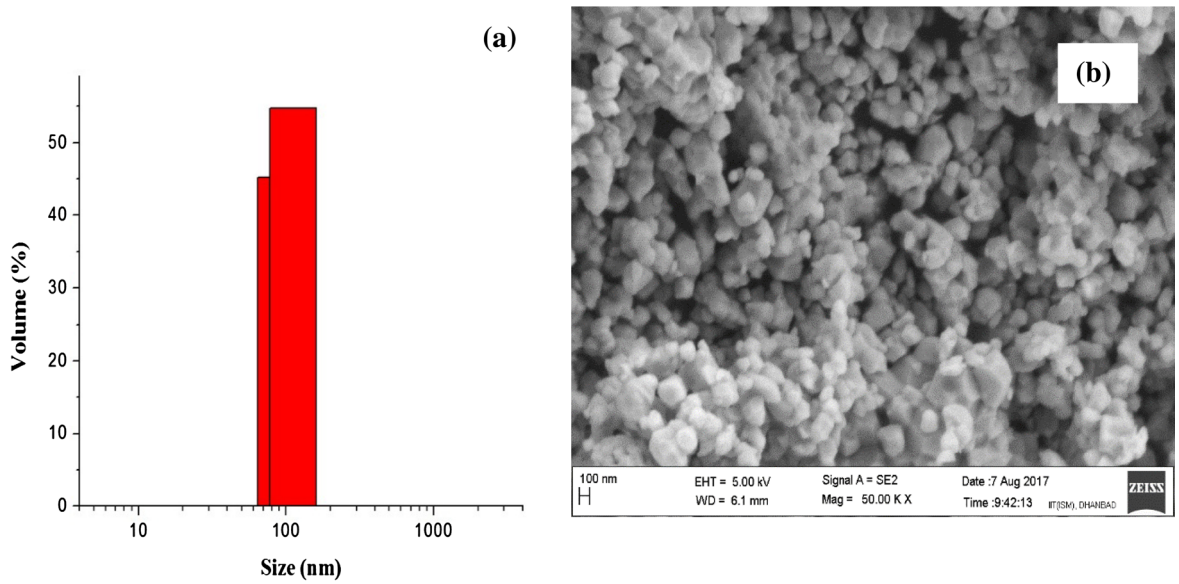

Fig. 1 **a** Dynamic light scattering analysis of γ-Al_2O_3 NPs, **b** FESEM of γ-Al_2O_3 NPs

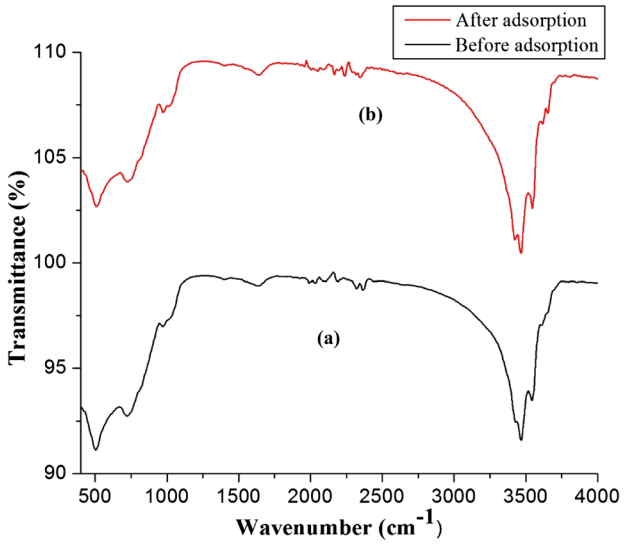

Fig. 2 FTIR spectra of **a** pure γ-Al_2O_3 NPs before adsorption and **b** after adsorption of As(III)

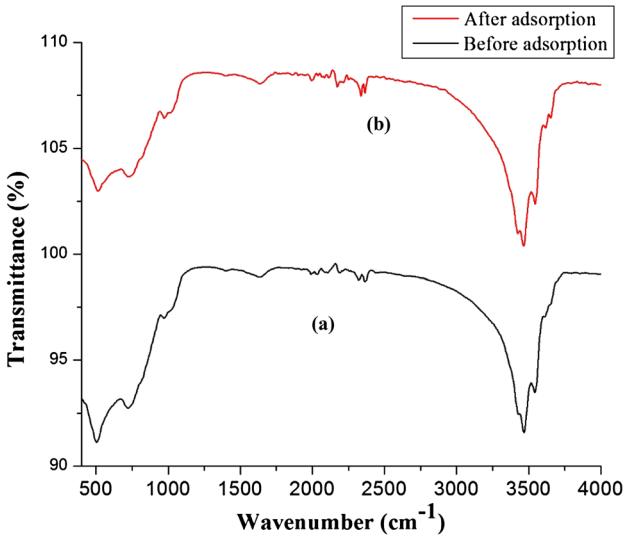

Fig. 3 FTIR spectra of **a** pure γ-Al_2O_3 NPs before adsorption and **b** after adsorption of As(V)

was 40 m^2/g as specified by the supplier. The pH_{ZPC} of the γ-alumina was found to be 7.9 (Fig. S4), which further confirmed that the surface of γ-alumina was positively charged below pH 7.9 which is consistent with previously reported studies by other researcher on alumina nanoparticles (such as Prabhakar and Samadder 2018). Figure 2 shows the FTIR spectra of pure and arsenite-loaded γ-Al_2O_3 NPs for functional group identification. A number of significant peaks bearing stretching vibration of –OH group can be observed between 3000 and 3600 cm^{-1} (Fig. 2). The weak peak of lattice water molecules was characterized at 1623 cm^{-1}. The appeared weak bands between 1100 and 1500 cm^{-1} corresponded to Al–O bands. The recognized bands of bending vibration, asymmetric stretching and symmetric stretching of the Al–O–Al bond were at 597, 735 and 987 cm^{-1}, respectively. No major shift in the peaks of untreated and arsenite-loaded γ-Al_2O_3 NPs was observed during FTIR analysis, which further confirmed that there was no chemical reaction between adsorbate and adsorbent. In case of arsenate adsorption using γ-Al_2O_3 NPs, there was slight shift in the range of wavenumber of 2000–2500 cm^{-1} and 500 cm^{-1} which preliminary indicated some minor and insignificant interaction between nanoparticles and arsenate (Fig. 3).

Batch parametric studies

Contact time

Contact time is vital parameter as it influences the expediency and its cost feasibility in pilot scale application. From Fig. 4a, it was evident that with the escalation in the equilibrium time from 10 to 120 min, removal efficiency increased from 65.74 to 91.77% for arsenite and for arsenate the removal percentage reached 97.69% from 69.84%. Beyond contact time of 120 min, no significant increase in the removal efficiency was observed for both the species due to saturation of the active sites of the nanoparticles. As can be seen from Fig. S5, as the time progressed, the equilibrium concentration and removal percentage decreased and became almost constant after 120 min. The variation of the percentage removal was negligible (less than 1%). Therefore, 120 min was considered as the optimum contact time for performing further experiments.

Stirring speed

The distribution of solute in the bulk solution is affected by stirring speed (Goswami et al. 2012). Development of the external boundary layer, which contributes the compactness between the adsorbent and adsorbate, also depends on the speed of agitation. The results represented that after agitating the samples at a stirring speed of 150 rpm, a negligible increase in the removal efficiency was obtained (Fig. 4b). This phenomenon can be interpreted as nano-sized particles of γ-Al_2O_3 were thoroughly and homogenously suspended in the solution that caused the rise in the adsorption rate with the rise in the agitation speed.

Initial arsenic concentration

The experimental results showed that with the increment in the initial arsenic concentration (50–400 µg/L), the equilibrium concentration increased from 3.62 to 53.12 µg/L for As(III) at initial As(III) concentration of 50 µg/L and

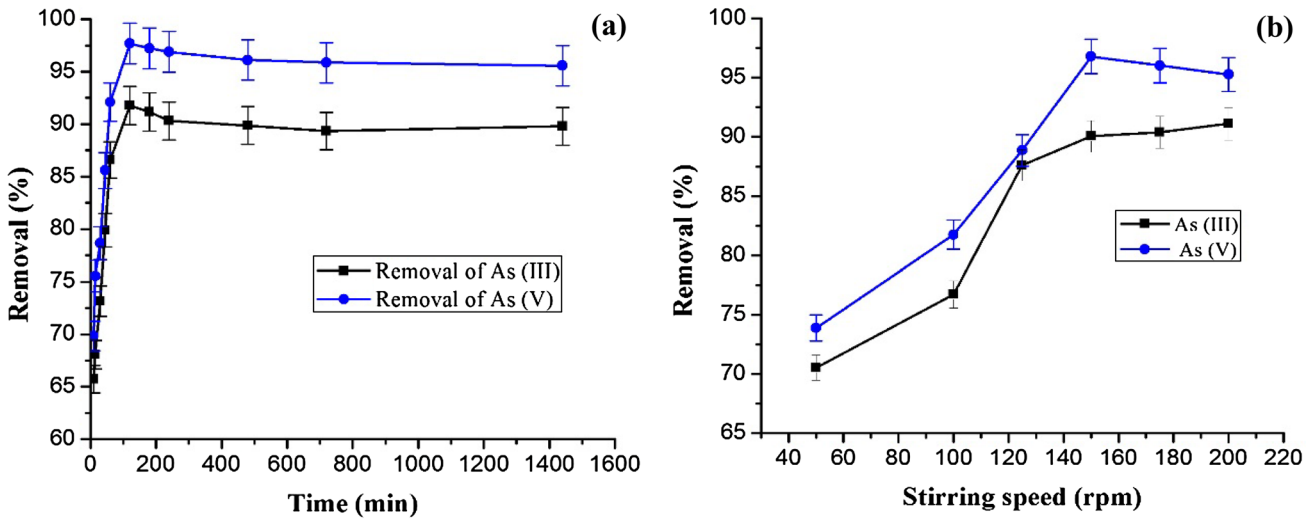

Fig. 4 **a** Effect of contact time on arsenic removal (experimental conditions: i.c—100 ppb, dose—0.5 g/L, pH—6.8, temp—298 K, contact time—10–1440 min, stirring speed—130 rpm) and **b** effect of stirring speed on arsenic removal (experimental conditions: i.c—100 ppb, dose—0.5 g/L, pH—6.8, temp—298 K, contact time—120 min for As(III) and As(V), stirring speed—50–200 rpm)

400 µg/L, respectively, and 0.45–28.08 µg/L or As(V) at initial As(V) concentration of 50 µg/L and 400 µg/L, respectively (Fig. S6). This phenomenon indicated that with increasing initial arsenic concentration, the number of active sites of the adsorbent fell short with a fixed amount of adsorbent dose to adsorb all the As(III) and As(V). A higher initial concentration provides an important driving force to overcome all the mass transfer resistance between the aqueous and solid phases of the pollutant, and thus, the uptake capacity increased with the equilibrium concentration (in other words with the initial arsenic concentration) of the arsenic species (Fig. 5a). For As(III), uptake capacity increased from 92.76 to 693.76 µg/g with the increase in the initial As(III) concentration from 50 to 400 µg/L. In the case of As(V) adsorption, the increment of uptake capacity was from 99.10 to 743.84 µg/g with the rise of initial arsenic concentration in the range of 50–400 µg/L. Removal was as high as 92.76% for arsenite and 99.1% for arsenate. With the increment in the arsenic concentrations, the adsorption efficiency kept on decreasing and reached a constant value at 300 µg/L with removal efficacy of 87.69% and 93.91% for arsenite and arsenate, respectively. On further rise in the initial arsenic concentration beyond 300 µg/L, there were nominal changes in the removal efficiency. Hence, initial concentration of 300 µg/L was taken as optimum value for both the arsenic species.

Adsorbent dose

To achieve a cost-efficient treatment system, evaluating the equilibrium value of the adsorbent dose is important. The results as illustrated in Fig. 5b represented that with increase in the dose (0.1–2 g/L), the uptake capacity kept on decreasing [2025.70–136.39 µg/g for As(III) and 2403.5–147.04 µg/g for As(V)]. With lower adsorbent dose, higher competition for the adsorbent's active sites led to higher uptake capacity and lower percentage removal. An expeditious increase in the removal efficacy from 67.52 to 92.07% for the dosages varying from 0.1 to 0.75 g/L for arsenite removal has been found. Similarly, for arsenate, the removal efficiency increased to 97.77% from 80.11% for the dosages varying between 0.1 and 0.5 g/L. With additional increase in the dosage, there was no significant increase in the removal, although the uptake capacity kept on decreasing with the increase in the adsorbent dose. Therefore, 0.75 g/L and 0.5 g/L were chosen as optimum adsorbent dose for arsenite and arsenate removal, respectively, and were used for further studies.

Effect of pH

pH is an essential parameter of adsorption study which affects the sorption capacity of the nano-adsorbents and regulates the feasibility of treatment method. The behaviour of the adsorbent in remediation of arsenite and arsenate was assessed over a wide range of pH of 2–12 (Fig. 5c) with optimized value of equilibrium time, stirring speed, initial arsenic concentration and adsorbent dose. Variation in removal percentage of arsenate was not significant up to pH 8. Arsenite remains as neutral species of H_3AsO_3 up to pH 9.17 (Chaudhry et al. 2016) and was less attracted by the electrostatic forces between arsenate and gamma-alumina. Occurrence of undissociated

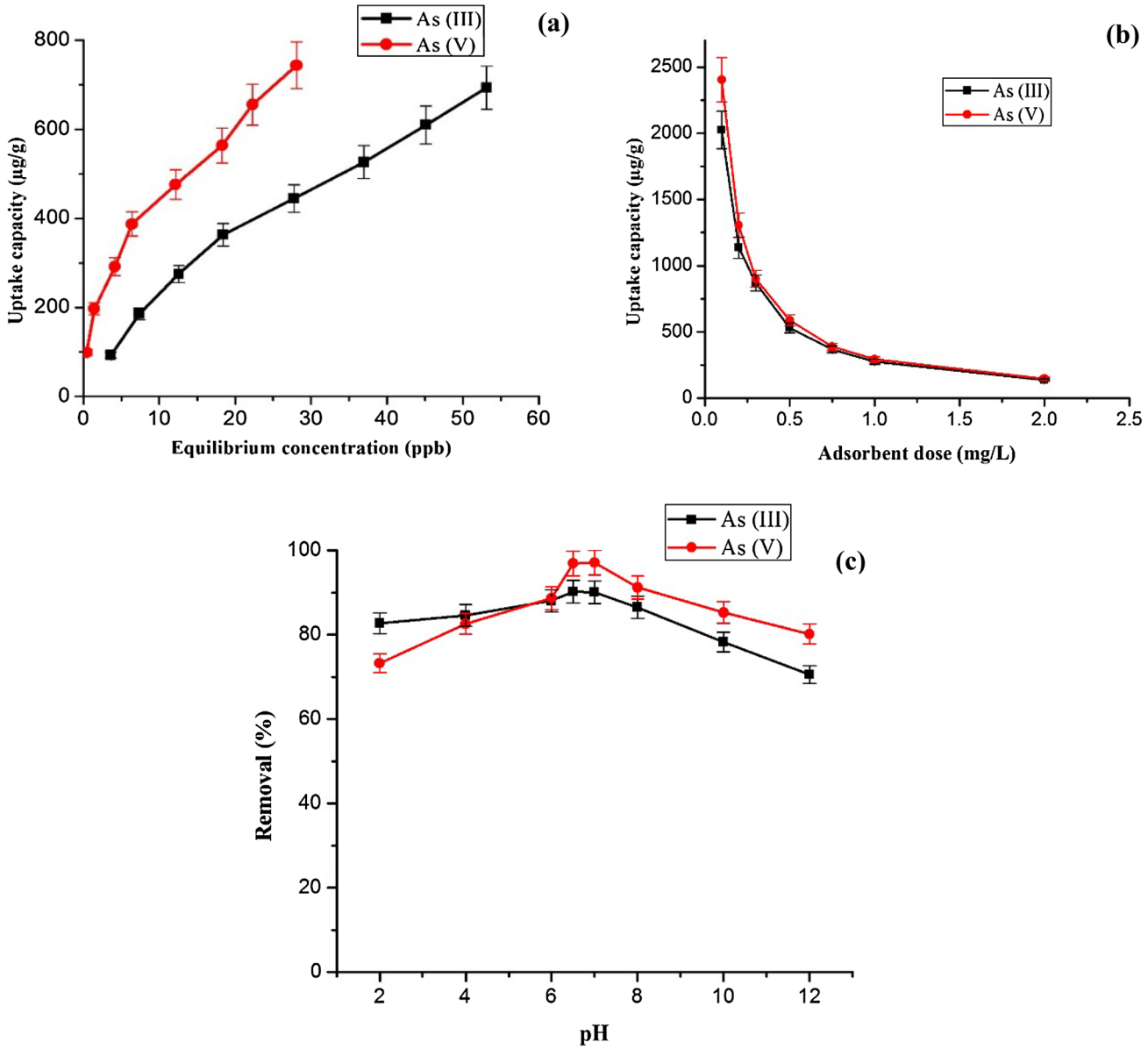

Fig. 5 **a** Effect of initial concentration on arsenic removal [experimental conditions: i.c—50–400 ppb, dose—0.5 g/L, pH—6.8, temp—298 K, contact time—120 min for As(III) and As(V), stirring speed—150 rpm for both As(III) and As(V)], **b** effect of adsorbent dose on arsenic removal [experimental conditions: i.c—300 ppb for both As(III) and As(V), dose: 0.1–2 g/L, pH—6.8, temp—298 K, contact time—120 min for As(III) and As(V), stirring speed—150 rpm for both As(III) and As(V)] and **c** effect of pH on arsenic removal [experimental conditions: i.c—300 ppb for both As(III) and As(V), dose—0.75 g/L for As(III) and 0.5 g/L for As(V), pH—2–12, temp—298 K, contact time—120 min for As(III) and As(V), stirring speed—150 rpm for both As(III) and As(V)]

form of arsenite for the wide range of pH values was the main reason for obtaining lesser removal using γ-Al_2O_3. $HAsO_4^{2-}$ and $H_2AsO_4^-$ were the dominant species of arsenate in pH range of 2–7, whereas at lower pH, adsorbent surface was highly positive which led to higher removal of arsenate by the involvement of electrostatic attraction forces. The surface of the adsorbent became negatively charged at higher pH (greater than pH_{ZPC}), and removal was decreased sharply as a result of electrostatic repulsion between the arsenic species and alumina NPs. Higher OH^- concentration became competitive for the active sites also. Overall, the nano-adsorbent showed higher removal efficiency in neutral pH range. The natural pH (6.8) of the arsenic solution was nearly neutral. Therefore, further experiments were performed with unaltered pH of the arsenic solutions.

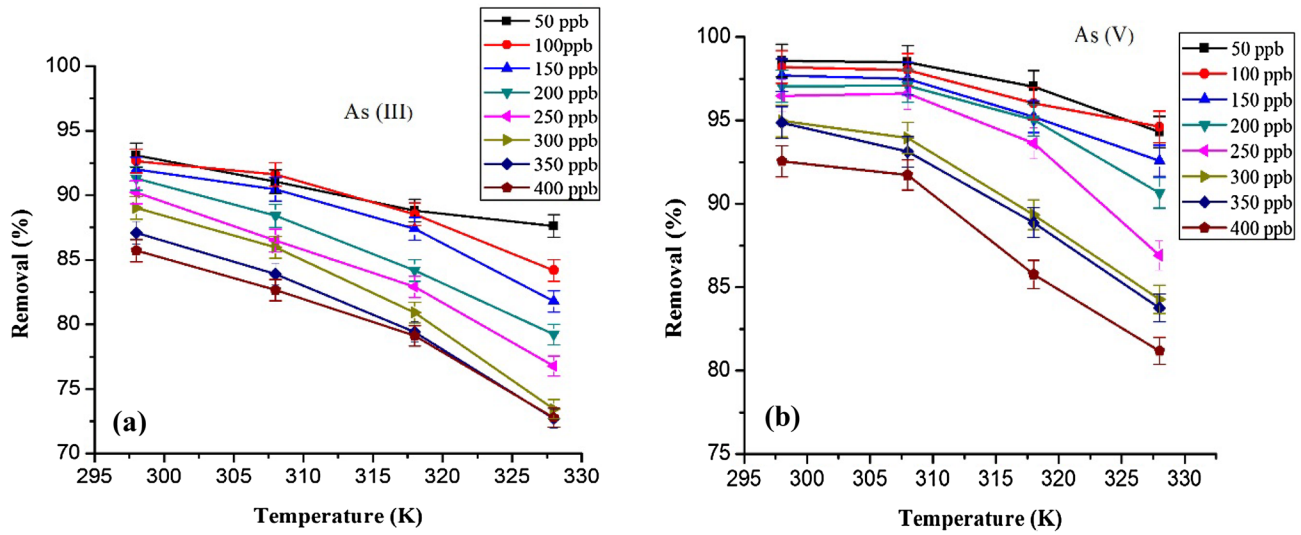

Fig. 6 **a** Effect of temperature on As(III) removal and **b** effect of temperature on As(V) removal (experimental conditions: i.c—300 ppb, dose—0.75 g/L for As(III) and 0.5 g/L for As(V) for, pH—6.8, temp—298–328 K, contact time—120 min, stirring speed—150 rpm)

Temperature

Temperature is a crucial parameter that influences the adsorption of contaminant. In order to discern the effect of temperature, tests were carried out at four different temperatures (298 K, 308 K, 318 K and 328 K). The samples of varying concentration of 50–400 µg/L were agitated for a predetermined contact time of 120 min with optimum conditions of dose and pH. From Fig. 6a, b, it can be seen that along with the rise in temperature, the removal percentage kept on decreasing. The highest performance in removal was achieved at 298 K for both the arsenic species. The results exhibited that low temperature was the favourable condition for efficient adsorption mechanism. The outcome of the current work implied the appropriateness of the developed method in natural condition. Furthermore, the results also illustrated that the system does not need any additional energy source to attain better removal efficiency; in other words, the system will surely lead to a cost-beneficial treatment approach.

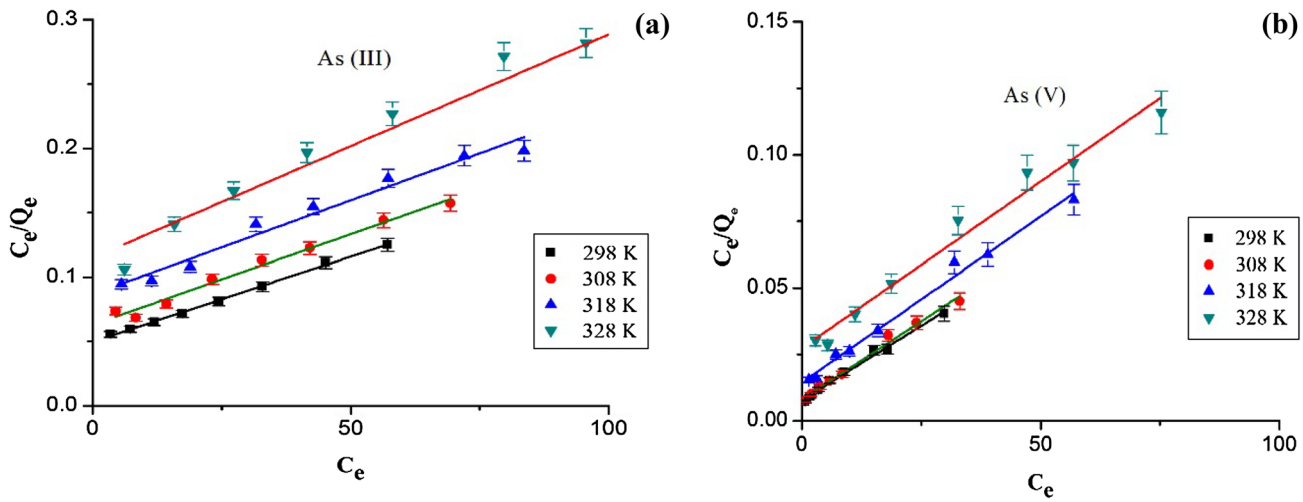

Fig. 7 **a** Langmuir isotherm model for As(III) adsorption and **b** effect of temperature on As(V) removal (experimental conditions: i.c—300 ppb, dose—0.5 g/L, pH—6.8, temp—298–328 K, contact time—120 min, stirring speed—150 rpm)

Table 1 Values of the adsorption isotherm parameters for arsenite and arsenate removal using γ-Al_2O_3 NPs

S. no.	Isotherm models	As(III)				As(V)			
		Temperature (K)				Temperature (K)			
		298 K	308 K	318 K	328 K	298 K	308 K	318 K	328 K
1.	*Langmuir isotherm*								
	Q_m (μg/g)	769.23	714.28	666.67	588.23	1000	833.33	775.10	724.63
	K_L (L/μg)	0.026	0.022	0.017	0.014	0.128	0.15	0.09	0.05
	R_L	0.43–0.08	0.47–0.10	0.47–0.10	0.58–0.15	0.135–0.019	0.11–0.016	0.18–0.02	0.28–0.04
	R^2	0.99	0.99	0.98	0.96	0.99	0.99	0.98	0.97
2.	*Freundlich isotherm*								
	K_f {(μg/g)/(μg/L)$^{1/n}$}	28.84	24.11	20.41	18.62	137.11	135.89	97.72	66.06
	n	1.42	1.44	1.44	1.56	1.856	1.941	1.96	1.839
	R^2	0.98	0.97	0.98	0.99	0.97	0.96	0.95	0.96
3.	*Dubinin–Radushkevich isotherm*								
	K (mol^2/kJ^2)	−4.48	−6.66	−9.13	−9.49	−0.374	−0.378	−0.94	−2.55
	Q_m	311.06	304.90	284.29	252.14	492.74	482.99	473.42	450.33
	E (kJ/mol)	0.33	0.27	0.23	0.22	1.156	1.15	0.729	0.44
	R^2	0.79	0.83	0.80	0.73	0.78	0.78	0.81	0.83
4.	*Temkin isotherm*								
	b_T	0.017	0.019	0.02	0.024	0.0139	0.015	0.016	0.0167
	A_T	0.357	0.286	0.233	0.208	1.839	1.83	1.06	0.55
	R^2	0.97	0.97	0.96	0.94	0.97	0.98	0.98	0.97

Isotherm studies

Langmuir isotherm The plot between C_e/Q_e and C_e gave the isotherm constants (Fig. 7). Table 1 represents the calculated values of isotherm parameters. The K_L values were 0.026 (298 K), 0.022 (308 K), 0.017 (318 K) and 0.014 (328 K) L/μg for arsenite adsorption. For arsenate adsorption, these values at four different temperatures in increasing order were 0.128, 0.15, 0.09 and 0.05 L/μg. The higher values of K_L for the removal of arsenate as compared to the arsenite removal confirmed the ease of adsorption process for the arsenate (Chaudhry et al. 2016). The maximum adsorption capacities (Q_m) were found as 769.23, 714.28, 666.67 and 588.23 μg/g for arsenite adsorption at four different temperatures, respectively, whereas the adsorption capacities for arsenate were observed as 1000, 833.33, 775.10 and 724.63 μg/g at the studied temperature range. The isotherm studies conducted at different temperature showed that adsorption was less favoured at high temperature. Therefore, maximum adsorption capacity of 769.23 μg/g and 1000 μg/g for arsenite and arsenate, respectively, will be taken into account. All other Q_m values obtained at three other temperatures are neglected. The maximum adsorption capacity obtained for arsenate removal was higher (1000 μg/g) than that of arsenite removal (769.23 μg/g), which in addition confirmed γ-alumina nanoparticles were more efficient for arsenate removal than that of arsenite.

For the present study, the R_L values were in the range of 0.08–0.58 for arsenite removal and for arsenate removal these were in the range of 0.019–0.28. However, the R_L values kept on increasing with the augmentation in temperature. The least value of R_L was observed at 298 K for both the arsenic species, which obviously showed that the mechanism was less suitable at higher temperature. Moreover, the R_L values obtained in the arsenate adsorption studies were smaller than that of arsenite adsorption, which further confirmed the capability of higher removal of arsenate using γ-Al_2O_3 NPs.

Freundlich isotherm The plot between log C_e and log Q_e (Fig. 8) provided K_f and n values correspondingly. It can be seen from Table 1 that K_f values were in the range of 18.62–28.84 and 66.06–137.11 [(μg/g)/(μg/L)$^{1/n}$] for arsenite and arsenate removal, respectively. Apparently, the removal was less favoured at higher temperatures as the values of K_f decreased with the rise in the temperature. Further, the "n" values in between 1 and 10 presented in Table 1 established favourable condition of adsorption (Prabhakar and Samadder 2018).

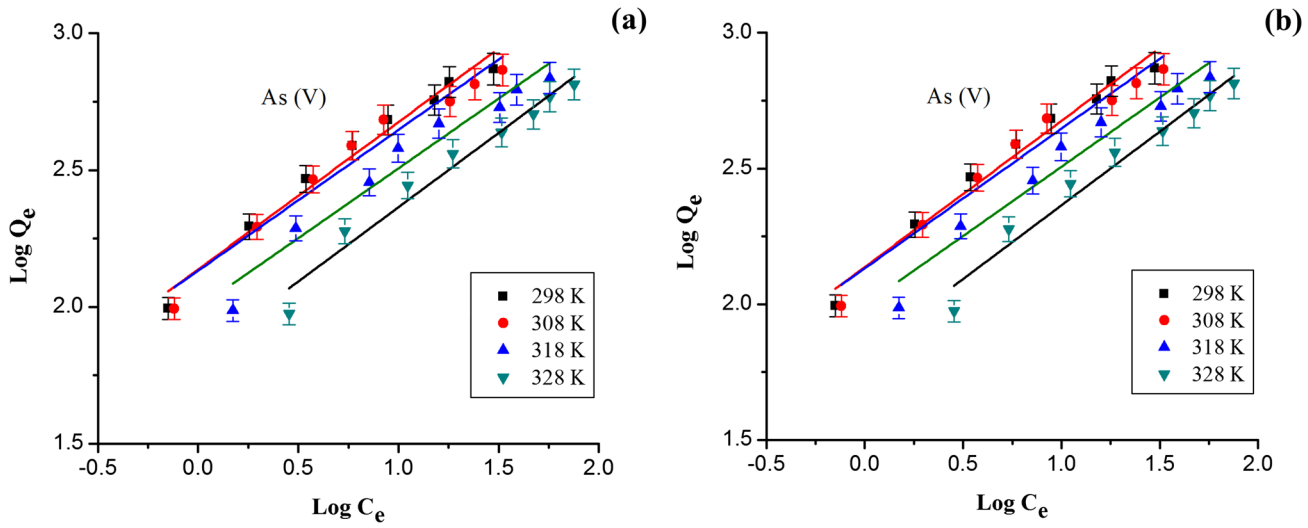

Fig. 8 **a** Freundlich isotherm model for As(III) adsorption and **b** Freundlich isotherm model for As(V) adsorption (experimental conditions for **a**, **b**: i.c—50–400 ppb, dose—0.5 g/L, pH—6.8, temp—298–328 K, contact time—120 min, stirring speed—150 rpm)

Dubinin–Radushkevich (D–R) isotherm Q_m and k were determined from the slope and intercept of the plot of ln Q_e and ε^2 as shown in Fig. S7. The observed values of theoretical saturation capacity at four different temperatures as stated above for arsenite and arsenate removal are depicted in Table 1. The mean sorption energy (E) values ranged from 0.22 to 0.33 kJ/mol and 0.44 to 1.156 kJ/mol for arsenite and arsenite adsorption, respectively. The values of E found lesser than 8 kJ/mol indicated that the adsorption process was predominantly a physical adsorption (Lunge et al. 2014) which was additionally confirmed by the results obtained from FTIR spectra.

Temkin isotherm A_T was found from the ln C_e and Q_e plot (Fig. S8). The A_T values as illustrated in Table 1 represent the binding energy between arsenic species and aluminium oxide nanoparticles and also implied arsenic-adsorbent interactions at the four different temperatures. The small changes in the b_T values in Table 1 showed less variation in the heat of adsorption at all four different temperatures for the removal of both the arsenic species. The smaller A_T values obtained during As(III) adsorption as compared to that of As(V) suggested that the binding of As(V) with γ-alumina NPs is more favourable than that of As(III) with γ-alumina NPs. Regression coefficient (R^2) approached unity as shown in Table 1, indicating applicability of Temkin isotherm model.

On the basis of proximity of the theoretical to experimental (Q_e) and R^2 values, it can be said that Langmuir isotherm was the governing isotherm model as compared to the other three applied isotherm models. The uptake capacities obtained from the Langmuir isotherm model for the present study were much higher than some recently reported studies on arsenic removal using any adsorbents. Chaudhry et al. (2016) reported 82.64 µg/g of uptake capacity for arsenite and 227 µg/g for arsenate removal using Fe(III)–Sn(IV) mixed binary oxide-coated sand. Prabhakar and Samadder (2018) reported maximum Langmuir uptake capacity of 500 µg/g for arsenite removal using alpha-alumina nanoparticles. Al Hamouz and Akintola (2017) found maximum uptake capacity using Langmuir isotherm of 169.5 µg/g for arsenate removal using aniline-based polymers. Altundoğan et al. (2002) reported maximum Langmuir uptake capacity of 6.86 µmol/g (513.95 µg/g at 25 °C) and 10.80 µmol/g (809.136 µg/g at 70 °C) for As(V) using raw red mud and the maximum adsorption capacity for As(V) adsorption obtained using activated red mud was 11.8 µmol/g (941.74 µg/g at 25 °C). Bentahar et al. (2016) found that maximum Langmuir adsorption capacities for As(V) removal using Moroccan clays were 678 µg/g and 561 µg/g using E-clay and A-clay, respectively. Arsenic adsorption depends on both specific surface area and the initial arsenic concentration. The present study exhibits a considerably high removal efficiency in the initial concentration range of arsenic that is often found in natural groundwater and normal condition without any external energy application. Column study can be designed on basis of the high adsorption capacity of γ-Al_2O_3 to remove both As(III) and As(V) from groundwater at field-scale approach at natural condition.

Kinetic modelling

Pseudo-first-order kinetics The values of k_1 and the theoretical Q_e were obtained from the curve of log (Q_e–Q_t) ver-

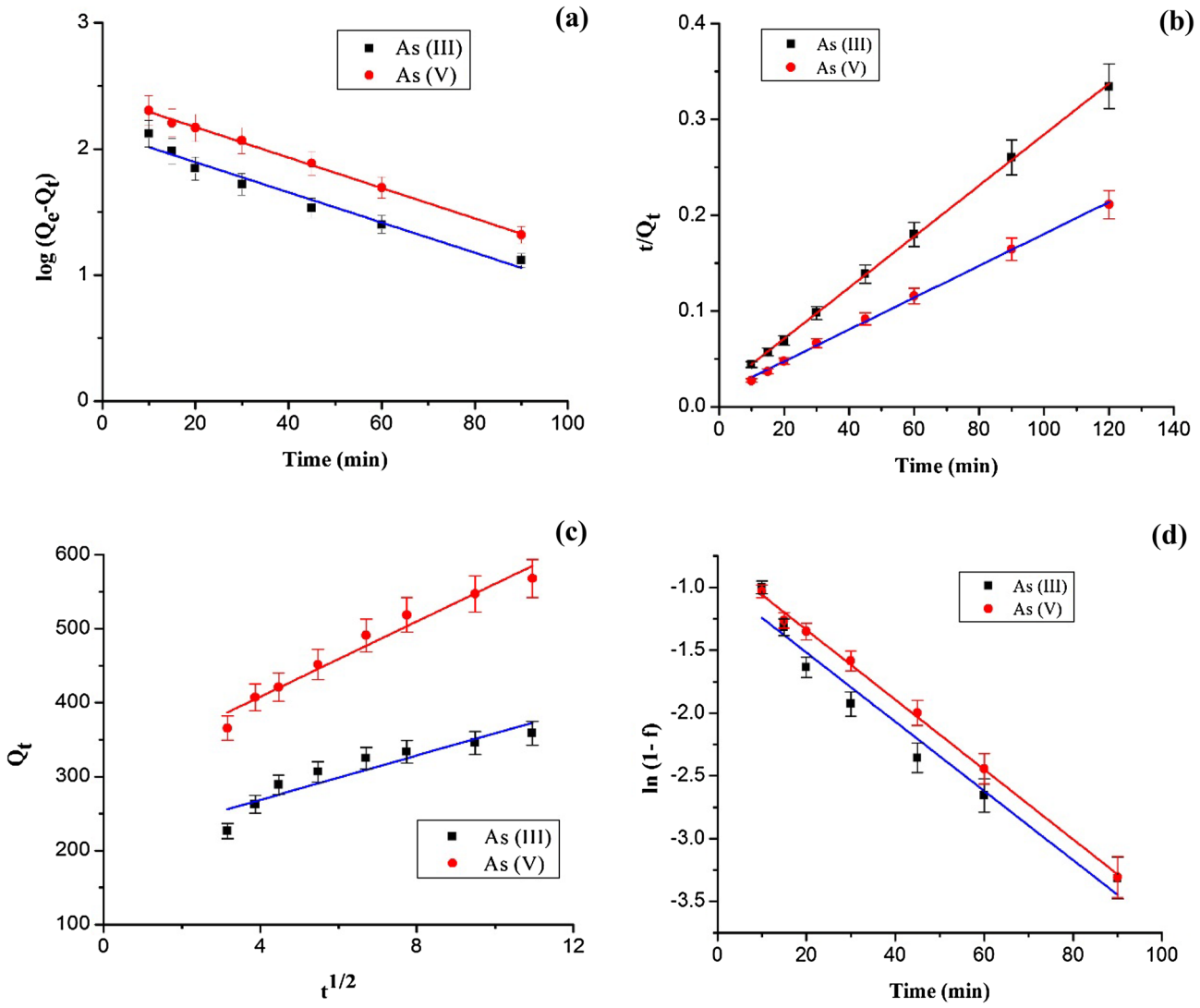

Fig. 9 **a** Pseudo-first-order kinetic model, **b** pseudo-second-order kinetic model, **c** intraparticle diffusion kinetic model and **d** liquid film kinetic model (experimental conditions: i.c—300 ppb, dose—0.75 g/L for As(III) adsorption and 0.5 g/L for As(V) adsorption, pH—6.8, temp—298 K, contact time—10–120 min, stirring speed—150 rpm)

Table 2 Values of the kinetic parameters for arsenite and arsenate adsorption using γ-Al_2O_3 NPs

S. no.	Arsenic species	Q_e (E) (μg/g)	Pseudo-first order			Pseudo-second order			
			k_1 (min^{-1})	Q_e (T) (μg/g)	R^2	k_2 (g/μg min)	Q_e (T) (μg/g)	h (μg/g min)	R^2
1.	As(III)	358.75	0.038	186.2	0.93	4.09×10^{-4}	370.37	56.10	0.99
2.	As(V)	568.08	0.042	398.10	0.90	2.06×10^{-4}	588.23	71.27	0.99

Q_e (E)—experimental adsorption capacity, Q_e (T)—theoretical adsorption capacity

sus time (t) as demonstrated in Fig. 9a. From Table 2, it can be seen that k_1 values were 0.038 min^{-1} and 0.042 min^{-1} at 298 K for arsenite and arsenate, respectively. Theoretical adsorption capacity Q_e (T) was significantly lower than the experimental Q_e (E). This applied model did not fit for the current study.

Pseudo-second-order kinetics k_2 was obtained from the graph of t/Q_t versus t (Fig. 9b). The value of k_2 was higher for arsenate adsorption as compared to the removal of arsenite (Table 2). The initial rate constant ($h = k_2 Q_e^2$) was found as 56.10 μg/g min for arsenite removal, and it was 71.27 μg/g min for arsenate removal. The h val-

ues were higher than k_2 which evidently recommended that adsorption was rapid at the beginning of the adsorption process (Prabhakar and Samadder 2018). Higher h values for arsenate removal suggested that adsorption of arsenate was more favoured than arsenite removal. It was observed that experimental Q_e values of 358.75 µg/g and 568.08 µg/g were approaching the theoretical values of Q_e (370.37 µg/g and 588.23 µg/g) for arsenite and arsenate removal, respectively (Table 2). Hence, on the root of proximity of the experimental and theoretical Q_e values, and R^2 values, it can be determined that pseudo-second-order model was the suitable model to explain the mechanism of arsenite and arsenate adsorption for the present study.

Different steps are involved in the process of adsorption such as film diffusion bulk diffusion, intraparticular diffusion and lastly attachment on the active pore spaces of an adsorbent (Khan et al. 2013). The inclusive rate of adsorption is regulated by the slowest rate-limiting step. The reaction rate might not depend on the mass action as this is comparatively a fast process in the case of physical adsorption; rather, adsorption depends either on intraparticular diffusion or on liquid film model (Zeldowitsch 1934). Hence, it is important to test the kinetic data using well-established mathematical models like intraparticular diffusion and liquid film model to explain the exact mechanism of adsorption.

Intraparticle diffusion The plot between Q_t and $t^{1/2}$ gave the value of intraparticle diffusion rate constant k_{id} (Fig. 9c). k_{id} values at 298 K were 15.02 µg/g $min^{1/2}$ and 25.46 µg/g $min^{1/2}$ for arsenite and arsenate, respectively (Table 3). The graph showed multilinear nature. This implied that movement between pores was not the rate-determining step during adsorption using γ-Al_2O_3 NPs. The higher values of intercepts were observed for both the arsenic species that suggested the involvement of the external boundary layer for the arsenic remediation (Khan et al. 2013).

Liquid film diffusion The multilinear and out of shape nature of intraparticle diffusion led to the development of liquid film diffusion for the current study. Hence, liquid film diffusion model was employed at 298 K. The straight line graph was obtained by plotting the graph between ln $(1-f)$ and t (Fig. 9d). The k_{fd} values were found as −0.0276 g/µg for arsenite and −0.0278 g/µg for arsenate (Table 3). The values of R^2 (0.96 for arsenite and 0.99 for arsenate) were higher than the pore diffusion that liquid film diffusion was a rate-regulating step for the current study.

Thermodynamic studies

Studies of the thermo-dynamic parameters were done to anticipate the mechanism of the arsenic removal using gamma-alumina. The parameters such as Gibb's free energy, standard enthalpy and entropy were calculated using Eqs. (14), (15) and (16) and are shown in Table 4.

$$\Delta G^\circ = -RT \ln K_c \tag{14}$$

$$\ln K_c = \frac{\Delta S^\circ}{R} - \frac{\Delta H^\circ}{RT} \tag{15}$$

$$\Delta G^\circ = \Delta H^\circ - T\Delta S^\circ \tag{16}$$

where ΔG°, ΔH°, R, ΔS° and K_c represent Gibb's free energy, standard enthalpy, universal gas constant, entropy and equilibrium constant correspondingly. The constant K_c was determined from the value of Q_e/C_e. ΔH° and ΔS° were considered from relation between ln K_c and $1/T$ (Fig. 10).

Table 3 Intraparticle and liquid film diffusion parameters for arsenite and arsenate adsorption using γ-Al_2O_3 NPs

S. no.	Arsenic species	Intraparticle diffusion			Liquid film diffusion		
		k_{id} (µg/g $min^{1/2}$)	Intercept	R^2	k_{fd} (g/µg)	Intercept	R^2
1.	As(III)	15.02	208.02	0.86	−0.0276	−0.966	0.96
2.	As(V)	25.46	306.18	0.96	−0.0278	−0.780	0.99

Table 4 Thermodynamic parameters of the adsorption process for arsenite and arsenate removal using γ-Al_2O_3 NPs

S. no.	Temperature	Thermodynamic constants					
		As(III)			As(V)		
		ΔG° (kJ/mol)	ΔH° (kJ/mol)	ΔS° (kJ/mol K)	ΔG° (kJ/mol)	ΔH° (kJ/mol)	ΔS° (kJ/mol K)
1.	298	−6.14	−29.12	−0.0077	−9.32	−35.55	−0.088
2.	308	−5.40			−8.44		
3.	318	−4.63			−7.56		
4.	328	−3.86			−6.68		

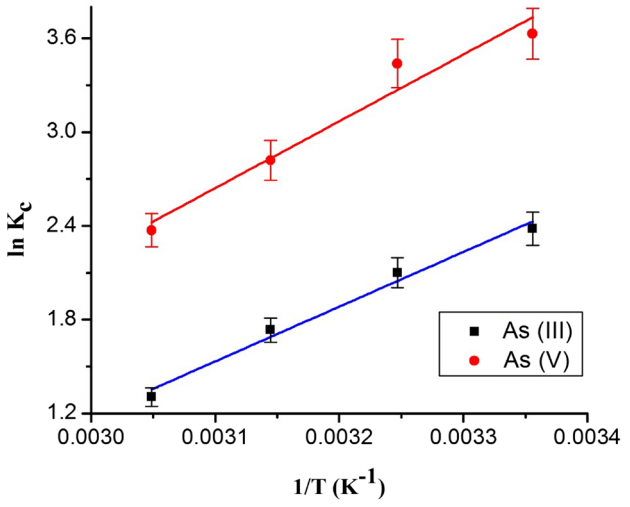

Fig. 10 Thermodynamic studies for determination of Gibb's free energy (Δ*G*°), change of standard enthalpy (Δ*H*°) and change of standard entropy (Δ*S*°) for As(III) and As(V) removal

Table 5 Characterization of collected groundwater

S. no.	Parameters	Observed values
1.	pH	6.8
2.	Electrical conductivity (EC) (μS/cm)	767
3.	Total hardness (mg/L as $CaCo_3$)	424
4.	Alkalinity (mg/L as $CaCo_3$)	208
5.	Total dissolved solids (mg/L)	458
6.	Nitrate (mg/L)	2.6
7.	Phosphate (mg/L)	0.12
8.	Chloride (mg/L)	24.96
Heavy metals concentration		
9.	Fe (mg/L)	0.115
10.	Zn (mg/L)	0.035
11.	Mn (mg/L)	0.3
12.	As (T) (μg/L)	169.4

The values of Δ*H*° for arsenite and arsenate removal were observed as − 29.12 kJ/mol and − 35.55 kJ/mol correspondingly. The Δ*H*° value was found negative which exhibited the exothermic performance of the interaction among arsenite, arsenate and γ-Al_2O_3 NPs. The values of Δ*H*° were well below 40 kJ/mol that further confirmed that both arsenite and arsenate removal was a physical adsorption mechanism. The values of Δ*S*° were obtained as − 0.077 kJ/mol K and − 0.088 kJ/mol K for removal of arsenite and arsenate, respectively. The negative values of Δ*S*° suggested that the entropy of the system reduced as a result of the increase in solute concentration at the surface of the nano-adsorbent. The mobility of the solute also decreased (arsenite and arsenate) in the aqueous solution. Gibb's free energy values obtained as − 6.14, − 5.40, − 4.63 and − 3.86 kJ/mol for adsorption of arsenite and for adsorption of arsenate these values were − 9.32, − 8.44, − 7.56 and − 6.68 kJ/mol at 298 K, 308 K, 318 K and 328 K, respectively. Spontaneous and favourable behaviour of the adsorption reaction was exhibited by the negative values of Δ*G*°. It was observed that with the rise in the temperature the magnitude of the free energy reduced, which further implied that efficient adsorption did not take place at higher temperature. It can also be concluded that the removal of both arsenite and arsenate was a physical adsorption process as the values of Δ*G*° ranged between − 20 and 0 kJ/mol (Nassar and Khatab 2016).

Effects of competing anions

It is now an established fact that the presence of different anions such as chloride (Cl^-), bicarbonate (HCO_3^-), sulphate (SO_4^{2-}), phosphate (PO_4^{2-}) and nitrate (NO_3^-) significantly affects the adsorption efficiency. The effects of these anions have been studied at high concentration (2000 μg/L) of these ions separately (Fig. S9). The concentration of both arsenic species was 300 μg/L. Optimum dose of gamma-alumina NPs (0.75 g/L for arsenite and 0.5 g/L for arsenate) was added to the arsenite and arsenate solutions, respectively, and the solutions were agitated using incubator shaker at 150 rpm for 2 h. It is elucidated from Fig. S9 that phosphate had the most adverse effect. Arsenite and arsenate removal was lowered down by 7.78% and 10.51%, respectively, by the presence of phosphate anion. Formation of surface complexation between phosphate anions and γ-Al_2O_3 NPs could be the possible reason for this event. Another reason could be the structural resemblances between arsenic and phosphate ions. The detrimental effects on percentage removal were then followed by the presence of sulphate on the removal of arsenic species. The presence of bicarbonate, chloride and nitrate anions had lesser impact on the removal process as compared to phosphate and sulphate anions.

Regeneration study of γ-Al_2O_3 NPs

To achieve a cost-efficient treatment system, regeneration of the used nano-adsorbents is very important and desirable. Regeneration was attained by increasing the pH of the arsenic-loaded nano-adsorbent above the pH_{ZPC} values of the γ-Al_2O_3 NPs. During the adsorption–desorption cycle with 0.5 N NaOH, rise in pH resulted in negative surface charge of the γ-Al_2O_3 NPs. Hence, desorption of the adsorbed arsenite occurred from the surface of the nano-adsorbent. The removal efficiency was decreased by 16.39% at the end of the fourth adsorption–desorption cycle (Fig. S10). After the fourth cycle of regeneration, remaining arsenic concentration was 17.66 μg/L, which was above the WHO

permissible limit (10 µg/L) of arsenic for drinking water. Therefore, the regenerative study was done up to fourth cycle only.

Application of γ-aluminium oxide nanoparticles in real arsenic-contaminated groundwater treatment

The experimental results of physicochemical and elemental analysis are reported in Table 5. The collected groundwater samples showed 169.4 µg/L of total arsenic concentration, which is quite higher than the permissible limit. The efficiency of γ-aluminium oxide nanoparticles for remediation of arsenic from the collected field samples was evaluated using the outcomes of batch adsorption studies. Considering the maximum adsorption capacity of the adsorbent, a fixed dose (8 mg) was added to 50 mL of the collected sample. Further, the sample was stirred at optimum contact time (2 h) to achieve equilibrium. After reaching the equilibrium time, remaining arsenic concentration in the sample was measured. The results showed that adsorption behaviour was concurrent with the competing anions study, and a consistent removal was achieved in the presence of naturally found anions. It was observed that γ-aluminium oxide nanoparticles satisfactorily removed (with removal efficiency of 94.63%) the arsenic well below the permissible limits. Hence, it is understood that the adsorbent γ-aluminium oxide nanoparticles have the potential for application in real arsenic-contaminated groundwater.

Conclusions

The present study illustrated that γ-Al_2O_3 NPs can be used as a potential nano-adsorbent that can remove both arsenite and arsenate from aqueous medium. More arsenate removal efficacy (as high as 94.96%) was achieved by adding lesser adsorbent dose of 0.5 g/L as compared to that of arsenite (89.02%) with dose of 0.75 g/L. Arsenite removal on the active pores of γ-Al_2O_3 was found as less pH dependent as compared to the adsorption of arsenate. However, the adsorption mechanism worked efficiently in remediation of both the arsenic species within drinking water pH range (6.5–8.5). This clearly suggested that a minimal or no pH adjustment is required while treating the water for arsenic. Adsorption isotherm modelling concluded that Langmuir was the optimum model for the present study. Time-dependent studies revealed that pseudo-second-order one was the governing kinetic model for removal of both the arsenic species. The thermodynamic data had shown the spontaneous and exothermic behaviour of the adsorption process. This behaviour will enabled the users to perform adsorption process in natural condition. It was also investigated that with equilibrium value of each parameter, γ-Al_2O_3 NPs can efficiently remove arsenite and arsenate below the WHO prescribed maximum limit of 10 µg/L with initial concentration of 100 µg/L for arsenite and 250 µg/L for arsenate. The removal was unaffected by the presence of competing anions like bicarbonate, chloride and nitrate. The anions phosphate and sulphate adversely affected the adsorption efficacy of the γ-Al_2O_3 NPs. The present study exhibited good regenerating efficiency of γ-Al_2O_3 NPs to achieve economically feasible treatment systems. γ-Al_2O_3 NPs worked satisfactorily for removal of arsenic from real arsenic-contaminated groundwater. Overall it can be said that the current study examined each aspect of adsorption mechanism for removal of arsenite and arsenate by the same nano-adsorbent and affirmed high removal efficiency with good regeneration capacity.

Acknowledgements The authors are sincerely grateful to the SERB-DST (Project No. SB/EMEQ-010/2014) for their financial support for the present research work. We would like to thank Department of ESE/IIT(ISM) Dhanbad, for providing all support needed. The authors would also like to acknowledge Indian Institute of Technology, Kharagpur, for allowing us to perform XRD analysis.

References

Al Hamouz OCS, Akintola OS (2017) Removal of lead and arsenic ions by a new series of aniline based polyamines. Process Saf Environ Prot 106:180–190

Allen SJ, Mckay G, Porter JF (2004) Adsorption isotherm models for basic dye adsorption by peat in single and binary component systems. J Colloid Interface Sci 280(2):322–333

Altundoğan HS, Altundoğan S, Tümen F, Bildik M (2002) Arsenic adsorption from aqueous solutions by activated red mud. Waste Manag 22(3):357–363

APHA (2012) Standards for examination of water and waste water, 22nd edn. American Public Health Association, America Water Works Association, Water Environment Federation, Washington

Bentahar Y, Hurel C, Draoui K, Khairoun S, Marmier N (2016) Adsorptive properties of Moroccan clays for the removal of arsenic(V) from aqueous solution. Appl Clay Sci 119:385–392

Bose P, Sharma A (2002) Role of iron in controlling speciation and mobilization of arsenic in subsurface environment. Water Res 36(19):4916–4926

Boyd GE, Adamson AW, Myers LS Jr (1947) The exchange adsorption of ions from aqueous solutions by organic zeolites. II. Kinetics1. J Am Chem Soc 69(11):2836–2848

Chakraborti D, Mukherjee SC, Pati S, Sengupta MK, Rahman MM, Chowdhury UK, Basu GK (2003) Arsenic groundwater contamination in Middle Ganga Plain, Bihar, India: a future danger? Environ Health Perspect 111(9):1194

Chakraborti D, Rahman MM, Chatterjee A, Das D, Das B, Nayak B, Sengupta MK (2016) Fate of over 480 million inhabitants living in arsenic and fluoride endemic Indian districts: magnitude, health,

socio-economic effects and mitigation approaches. J Trace Elem Med Biol 38:33–45
Chakraborti D, Das B, Rahman MM, Nayak B, Pal A, Sengupta MK, Saha KC (2017) Arsenic in groundwater of the Kolkata Municipal Corporation (KMC), India: critical review and modes of mitigation. Chemosphere 180:437–447
Chaudhry SA, Ahmed M, Siddiqui SI, Ahmed S (2016) Fe(III)–Sn(IV) mixed binary oxide-coated sand preparation and its use for the removal of arsenite and arsenate from water: application of isotherm, kinetic and thermodynamics. J Mol Liq 224:431–441
Chen CJ, Wang SL, Chiou JM, Tseng CH, Chiou HY, Hsueh YM, Lai MS (2007) Arsenic and diabetes and hypertension in human populations: a review. Toxicol Appl Pharmacol 222(3):298–304
Chowdhury UK, Biswas BK, Chowdhury TR, Samanta G, Mandal BK, Basu GC, Roy S (2000) Groundwater arsenic contamination in Bangladesh and West Bengal, India. Environ Health Perspect 108(5):393
Dutta PK, Ray AK, Sharma VK, Millero FJ (2004) Adsorption of arsenate and arsenite on titanium dioxide suspensions. J Colloid Interface Sci 278(2):270–275
EPA (2000) Regulations on the disposal of arsenic residuals from drinking water treatment plants. Office of Research and Development, U.S. EPA (EPA/600/R-00/025). http://www.epa.gov/ORD/WebPubs/residuals/index.htm
Garelick H, Jones H, Dybowska A, Valsami-Jones E (2009) Arsenic pollution sources. In: Whitacre DM (ed) Reviews of environmental contamination, vol 197. Springer, New York, pp 17–60
Giles DE, Mohapatra M, Issa TB, Anand S, Singh P (2011) Iron and aluminium based adsorption strategies for removing arsenic from water. J Environ Manag 92(12):3011–3022
Goswami A, Raul PK, Purkait MK (2012) Arsenic adsorption using copper(II) oxide nanoparticles. Chem Eng Res Des 90(9):1387–1396
Hansen HK, Núñez P, Grandon R (2006) Electrocoagulation as a remediation tool for wastewaters containing arsenic. Miner Eng 19(5):521–524
Ho YS, McKay G (1998) The kinetics of sorption of basic dyes from aqueous solution by sphagnum moss peat. Can J Chem Eng 76(4):822–827
Inaba K, Haga M, Ueda K, Itoh A, Takemoto T, Yoshikawa H (2016) New adsorbent for removal of inorganic arsenic(III) from groundwater. Chem Lett 46(1):58–60
Khan TA, Chaudhry SA, Ali I (2013) Thermodynamic and kinetic studies of Arsenate removal from water by zirconium oxide-coated marine sand. Environ Sci Pollut Res 20(8):5425–5440
Kim Y, Kim C, Choi I, Rengaraj S, Yi J (2004) Arsenic removal using mesoporous alumina prepared via a templating method. Environ Sci Technol 38(3):924–931
Kim DH, Kim KW, Cho J (2006) Removal and transport mechanisms of arsenics in UF and NF membrane processes. J Water Health 4(2):215–223
Kumar E, Bhatnagar A, Kumar U, Sillanpää M (2011) Defluoridation from aqueous solutions by nano-alumina: characterization and sorption studies. J Hazard Mater 186(2):1042–1049
Lata S, Samadder SR (2016) Removal of arsenic from water using nano adsorbents and challenges: a review. J Environ Manag 166:387–406
Leupin OX, Hug SJ (2005) Oxidation and removal of arsenic(III) from aerated groundwater by filtration through sand and zero-valent iron. Water Res 39(9):1729–1740
Lin SH, Juang RS (2002) Heavy metal removal from water by sorption using surfactant-modified montmorillonite. J Hazard Mater 92(3):315–326
Lunge S, Singh S, Sinha A (2014) Magnetic iron oxide (Fe_3O_4) nanoparticles from tea waste for arsenic removal. J Magn Magn Mater 356:21–31
Mazumder DNG, Haque R, Ghosh N, De BK, Santra A, Chakraborti D, Smith AH (2000) Arsenic in drinking water and the prevalence of respiratory effects in West Bengal, India. Int J Epidemiol 29(6):1047–1052
Mukherjee SC, Rahman MM, Chowdhury UK, Sengupta MK, Lodh D, Chanda CR, Chakraborti D (2003) Neuropathy in arsenic toxicity from groundwater arsenic contamination in West Bengal, India. J Environ Sci Health, Part A 38(1):165–183
Mukherjee SC, Saha KC, Pati S, Dutta RN, Rahman MM, Sengupta MK, Nayak B (2005) Murshidabad—one of the nine groundwater arsenic-affected districts of West Bengal, India. Part II: dermatological, neurological, and obstetric findings. Clin Toxicol 43(7):835–848
Murcott S (2012) Arsenic contamination in the world. IWA Publishing, London
Nassar MY, Khatab M (2016) Cobalt ferrite nanoparticles via a template-free hydrothermal route as an efficient nano-adsorbent for potential textile dye removal. RSC Adv 6(83):79688–79705
Nassar MY, Mohamed TY, Ahmed IS, Samir I (2017) MgO nanostructure via a sol–gel combustion synthesis method using different fuels: an efficient nano-adsorbent for the removal of some anionic textile dyes. J Mol Liq 225:730–740
Naujokas MF, Anderson B, Ahsan H, Aposhian HV, Graziano JH, Thompson C, Suk WA (2013) The broad scope of health effects from chronic arsenic exposure: update on a worldwide public health problem. Environ Health Perspect 121(3):295
Ning RY (2002) Arsenic removal by reverse osmosis. Desalination 143(3):237–241
Owlad M, Aroua MK, Daud WAW, Baroutian S (2009) Removal of hexavalent chromium-contaminated water and wastewater: a review. Water Air Soil Pollut 200(1–4):59–77
Patra AK, Dutta A, Bhaumik A (2012) Self-assembled mesoporous γ-Al_2O_3 spherical nanoparticles and their efficiency for the removal of arsenic from water. J Hazard Mater 201:170–177
Ponder SM, Darab JG, Bucher J, Caulder D, Craig I, Davis L, Shuh DK (2001) Surface chemistry and electrochemistry of supported zerovalent iron nanoparticles in the remediation of aqueous metal contaminants. Chem Mater 13(2):479–486
Prabhakar R, Samadder SR (2018) Low cost and easy synthesis of aluminium oxide nanoparticles for arsenite removal from groundwater: a complete batch study. J Mol Liq 250:192–201
Rahman MM, Chowdhury UK, Mukherjee SC, Mondal BK, Paul K, Lodh D, Roy S (2001) Chronic arsenic toxicity in Bangladesh and West Bengal, India—a review and commentary. J Toxicol Clin Toxicol 39(7):683–700
Rahman MM, Ng JC, Naidu R (2009) Chronic exposure of arsenic via drinking water and its adverse health impacts on humans. Environ Geochem Health 31(1):189–200
Roy PK, Majumder A, Banerjee G, Roy MB, Pal S, Mazumdar A (2015) Removal of arsenic from drinking water using dual treatment process. Clean Technol Environ Policy 17(4):1065–1076
Sharma YC, Srivastava V, Singh VK, Kaul SN, Weng CH (2009) Nanoadsorbents for the removal of metallic pollutants from water and wastewater. Environ Technol 30(6):583–609
Smith AH, Lopipero PA, Bates MN, Steinmaus CM (2002) Arsenic epidemiology and drinking water standards. Science 296(5576):2145–2146
Temkin MJ, Pyzhev V (1940) Recent modifications to Langmuir isotherms. Acta Phys Chim Sin 12:217–222

Tofik AS, Taddesse AM, Tesfahun KT, Girma GG (2016) Fe–Al binary oxide nanosorbent: synthesis, characterization and phosphate sorption property. J Environ Chem Eng 4(2):2458–2468

Wang CH, Hsiao CK, Chen CL, Hsu LI, Chiou HY, Chen SY, Hsueh Y-M, Wu M-M, Chen CJ (2007) A review of the epidemiologic literature on the role of environmental arsenic exposure and cardiovascular diseases. Toxicol Appl Pharmacol 222(3):315–326

Weber TW, Chakravorti RK (1974) Pore and solid diffusion models for fixed-bed adsorbers. AIChE J 20(2):228–238

Weber WJ, Morris JC (1963) Kinetics of adsorption on carbon from solution. J Sanit Eng Div 89(2):31–60

Wen Z, Zhang Y, Dai C, Chen B, Guo S, Yu H, Wu D (2014) Synthesis of ordered mesoporous iron manganese bimetal oxides for arsenic removal from aqueous solutions. Microporous Mesoporous Mater 200:235–244

Zeldowitsch J (1934) The catalytic oxidation of carbon monoxide on manganese dioxide. Acta Physicochim URSS 1:364–449